

# Reaction-drift-diffusion models from master equations: application to material defects

Thomas D Swinburne\*

*Université Aix-Marseille, CNRS, CINaM UMR 7325, Campus de Luminy, 13288 Marseille, France*

Danny Perez

*Theoretical Division T-1, Los Alamos National Laboratory, Los Alamos, NM, 87545, USA*

(Dated: October 29, 2021)

We present a general method to produce well-conditioned continuum reaction-drift-diffusion equations directly from master equations on a discrete, periodic state space. We assume the underlying data to be kinetic Monte Carlo models (i.e., continuous-time Markov chains) produced from atomic sampling of point defects in locally periodic environments, such as perfect lattices, ordered surface structures or dislocation cores, possibly under the influence of a slowly varying external field. Our approach also applies to any discrete, periodic Markov chain. The analysis identifies a previously omitted non-equilibrium drift term, present even in the absence of external forces, which can compete in magnitude with the reaction rates, thus being essential to correctly capture the kinetics. To remove fast modes which hinder time integration, we use a generalized Bloch relation to efficiently calculate the eigenspectrum of the master equation. A well conditioned continuum equation then emerges by searching for spectral gaps in the long wavelength limit, using an established kinetic clustering algorithm (e.g., PCCA+) to define a proper reduced state space.

Multiscale materials modeling is founded on the principle that atomic mechanisms at the nanoscale can be ‘coarse-grained’ for use in computationally efficient models that reach the mesoscale and beyond<sup>1–4</sup>. As these mechanisms are routinely of outstanding complexity<sup>5–9</sup>, they must first be discovered using the best available model of atomic cohesion (either using first principle methods such as density functional theory, or with semi-empirical interatomic potentials) that computational resources allow. Given a cohesive model, the conceptually simplest approach is to generate a molecular dynamics trajectory of the system under study and record transition events. However, as is well known, the constraint of serial time integration means that trajectories generated with molecular dynamics are limited to sub-microsecond timescales, often insufficient to observe the rare, thermally activated mechanisms that control the drift and diffusion of defects such as vacancy/interstitial clusters, impurity elements or adatom islands. This can prevent the accurate up-scaling of atomistic information into accurate continuum transport equations.

Over the last three decades a variety of approaches have been developed to overcome the timescale issue, including unbiased dynamic<sup>8,10?–16</sup> or static<sup>9,17,18</sup> sampling approaches. In the thermally activated regime, any system is extremely likely to thermalize in a local energy minima before escaping, giving a well defined separation of timescales between vibrations and transitions. In this limit, the atomic dynamics can be mapped to a continuous time, discrete state Markov chain<sup>19</sup>, which provides the theoretical basis of off-lattice, or atomistic kinetic Monte Carlo (akMC) methods<sup>20</sup>, up to an error exponentially small in the timescale separation<sup>21</sup>. We have employed this rigorous connection in our massively parallel sampling scheme TAMMBER<sup>15,16,22</sup> (available at

[github.com/tomswinburne/tammer](https://github.com/tomswinburne/tammer)), which optimally manages many thousands of molecular dynamics ‘workers’ to rapidly discover migration pathways of complex defects, with a novel Bayesian metric of sampling completeness which can be used to assign well defined uncertainty bounds on the resulting akMC model. Further discussion of TAMMBER can be found in a recent review<sup>23</sup>.

The coarse-graining of molecular dynamics to a Markov chain/akMC representation is thus well established, with a firm theoretical grounding. However, for all but the most simple defects, the corresponding akMC model can be prohibitively cumbersome, with a large number of states and huge differences between the fastest and slowest transition rates, requiring the use of advanced time-stepping schemes<sup>24,25</sup>. In addition, whilst the abstract, discrete state space of akMC is sufficiently general to allow a formal connection to molecular dynamics, it is clearly unsuitable for mesoscale methods such as cluster dynamics<sup>26–28</sup>, object kinetic Monte Carlo<sup>29–31</sup> or phase field models<sup>32,33</sup>, which require a computationally efficient *continuum* representation. This is particularly relevant for the growing number of approaches that couple point defect dynamics (through a reaction-diffusion equation representation) to dislocation dynamics<sup>34–36</sup> or crystal plasticity models<sup>37</sup>, essential for the modeling of irradiation-induced changes in material properties that are central to nuclear materials science<sup>38,39</sup>. As a result, coarse-graining to the mesoscale, either from akMC models or molecular dynamics observations, is typically an *ad hoc* phenomenological approach, requiring significant end-user expertise to ensure accuracy.

In this paper, we propose a data-driven approach to coarse-grain akMC models into reaction-diffusion equations. Following all rigorous coarse-graining schemes<sup>40</sup>,

we exploit separations of timescales in the model dynamics, here manifest as a gap in the eigenspectrum of the akMC master equation. Compressing the state space to retain only the slow modes then incurs an error exponentially small with respect to the size of the gap<sup>21</sup>. If a sufficiently large gap can be found, it is therefore simple to obtain an accurate yet dramatically simplified model that allows for efficient time-integration at the continuum scale.

A simple example of a master equation with a spectral gap is that of ‘super-basin-to-super-basin’ dynamics, where a periodically repeating group of states have much faster in-group transitions than between-group transitions. This could correspond, e.g., to the evolution of a cluster of point defects such that diffusion is slow compared to internal shape fluctuations, in an otherwise periodic crystal. A spectral gap then exists which justifies the local equilibrium approximation within each group. We show below this reduces the full master equation to a simple Brownian particle with an anisotropic diffusivity, with a spatial resolution limited to the lattice constant. However, in many settings, the eigenspectrum does not possess a spectral gap, implying that a rigorous coarse-graining procedure is not possible. In addition, computation of the eigenspectrum can present significant numerical issues. We propose a solution, first employing Bloch’s theorem to efficiently evaluate the reciprocal-space eigenspectrum of periodic master equations. We then identify regions of reciprocal space where a spectral gap exists, and truncate the short-wavelength modes above the gap, yielding an efficient, coarse-grained model at the expense of a reduced spatial resolution, generalizing the simple local equilibrium case.

The paper is structured as follows. We define the master equation for an isolated defect under periodic translation symmetries in section II and derive the continuum limit. In section III we show how the formally infinite dimension eigenvalue problem can be cast in a form reminiscent of the Kohn-Sham equations<sup>41</sup>, requiring only the diagonalization of a small rate matrix over a  $\mathbf{k}$ -space grid, naturally indexing eigenmodes by their spatial frequency and ‘band’. In III B the master equation is coarse-grained by leveraging timescale separations in the eigenvalue spectrum. As continuum equations operate in the limit of slow spatial variation, we need only look for timescale separations in this limit, significantly widening the range of systems to which such an approach can be applied. The number of below-gap ‘bands’ naturally defines the dimension of the reduced state space; the reduced states themselves are determined using the PCCA+ method<sup>42,43</sup>, an established kinetic clustering algorithm from the biochemical community<sup>40</sup>. Our approach, which provides simple reduced models for mesoscale simulations, is demonstrated on illustrative toy problems in IV. Application to real systems found in atomistic sampling will be the subject of future work.

Environment	Translation set $\mathcal{T}$
Bulk crystal	26 vectors to adjacent unit cells
Surfaces	8 vectors normal to plane
Grain boundaries	8 vectors of coincidence site lattice
Dislocations	2 vectors $\{\mathbf{d}, -\mathbf{d}\}$ along dislocation line

TABLE I. Common environments and corresponding set  $\mathcal{T}$  of translation vectors for point defects in crystals. Forward and backward directions are distinguishable, meaning  $\sum_{\mathcal{T}} \mathbf{d} = \mathbf{0}$ .

## I. ATOMIC SAMPLING IN LOCALLY PERIODIC ENVIRONMENTS

In this study, we focus on the kinetics of point defects in a range of *locally* periodic geometries, such that the local minima and saddle point configurations are invariant under translations generated by some primitive set of translations  $\mathcal{T}$ , formed from linear combinations of primitive lattice vectors  $\mathbf{a}_0, \mathbf{a}_1, \mathbf{a}_2$ . Examples of translation sets  $\mathcal{T}$  for common microstructural environments, such as surfaces, near dislocation lines or in the bulk crystal, are shown in table I. In this way, we can build exact master equations under the assumption of periodic translation symmetry, which yield a continuum governing equation with local differential operators.

This approach can produce local kinetic models for use in more complex microstructures, retaining sufficient complexity to exhibit a rich range of behaviors, including internal transitions (that can significantly affect mobility<sup>6,16</sup>), spontaneous disassociation<sup>15</sup>, or interaction with existing microstructural features such as dislocations or grain boundaries.

We note that these symmetries still hold in the presence of long-range external stresses that can be considered slowly varying, such as elastic interactions<sup>44</sup>, a point we return to below.

## II. THE MASTER EQUATION

To produce a master equation for a translation-symmetric system, under no external driving forces, we first index each unit cell by a three dimensional discrete lattice position  $\mathbf{x}_{\mathbf{n}} = \sum_{\alpha} n_{\alpha} \mathbf{a}_{\alpha}$ , where  $\mathbf{n} = [n_0, n_1, n_2]$  is an integer vector. The occupation probabilities for the  $M$  states in a cell at  $\mathbf{x}_{\mathbf{n}}$  are contained in a vector  $\mathbf{p}(\mathbf{x}_{\mathbf{n}}) \in \mathbb{R}^M$ , normalized such that  $\sum_{\mathbf{n}} \mathbf{1} \cdot \mathbf{p}(\mathbf{x}_{\mathbf{n}}) = 1$ , where  $\mathbf{1} = [1, 1, 1, \dots]$ .

Transition rates between states in the same cell are contained in a matrix  $\mathbf{Q}(\mathbf{0})$ , with intercell transition rates matrices  $\mathbf{Q}(\mathbf{d})$  for each  $\mathbf{d} \in \mathcal{T}$ . With these definitions, the master equation writes

$$\frac{d}{dt} \mathbf{p}(\mathbf{x}_{\mathbf{n}}, t) = [\mathbf{Q}(\mathbf{0}) - \mathbf{R}] \mathbf{p}(\mathbf{x}_{\mathbf{n}}, t) + \sum_{\mathbf{d} \in \mathcal{T}} \mathbf{Q}(\mathbf{d}) \mathbf{p}(\mathbf{x}_{\mathbf{n}} + \mathbf{d}, t), \quad (1)$$

where the diagonal matrix  $\mathbf{R}$  contains the total escape rate from each state, ensuring probability is conserved, with elements

$$[\mathbf{R}]_{ij} = \delta_{ij} \left[ \mathbf{1}^\top \mathbf{Q}(\mathbf{0}) + \sum_{\mathbf{d} \in \mathcal{T}} \mathbf{1}^\top \mathbf{Q}(\mathbf{d}) \right]_j. \quad (2)$$

As we use transition state theory, transition rates  $k_{ji}$  satisfy detailed balance<sup>45</sup> such that  $k_{ij}\pi_j = k_{ji}\pi_i$ , where  $\pi_i$  is the (un-normalized) equilibrium occupation probability for state  $i$ . With a diagonal  $M \times M$  matrix  $[\mathbf{\Pi}]_{ij} = \delta_{ij}\pi_i$ , this implies

$$\mathbf{Q}(\mathbf{d})\mathbf{\Pi} = \mathbf{\Pi}\mathbf{Q}(-\mathbf{d})^\top, \quad (3)$$

with  $\mathbf{Q}(\mathbf{0})\mathbf{\Pi} = \mathbf{\Pi}\mathbf{Q}(\mathbf{0})^\top$  being a special case with  $\mathbf{d} = \mathbf{0}$ . The steady state distribution therefore reads

$$\lim_{t \rightarrow \infty} \mathbf{p}(\mathbf{x}_n, t) = \left( \prod_{\alpha} N_{\alpha} \right)^{-1} \hat{\boldsymbol{\pi}}, \quad (4)$$

where  $N_{\alpha}$  is the total number of cells in each primitive direction and  $\hat{\boldsymbol{\pi}}$  is the cell normalized Boltzmann distribution.

### 1. External driving force

In the presence of a constant external driving force  $\mathbf{f}$ , typically due to a slowly varying stress gradient or an external electric field for charged defects, the detailed balance equation is modified to become

$$\mathbf{Q}(\mathbf{d}, \mathbf{f})\mathbf{\Pi} \exp(\beta \mathbf{d} \cdot \mathbf{f}) = \mathbf{\Pi}\mathbf{Q}(-\mathbf{d}, \mathbf{f})^\top, \quad (5)$$

where  $\beta = 1/k_B T$ ,  $\mathbf{Q}(\mathbf{d}, \mathbf{f})$  are modified rate matrices and  $\mathbf{d} \cdot \mathbf{f}$  is the additional energy difference between initial and final states due to  $\mathbf{f}$ . The steady state distribution becomes

$$\lim_{t \rightarrow \infty} \mathbf{p}(\mathbf{x}_n, t) = \left( \prod_{\alpha} \frac{1 - e^{-\beta \mathbf{a}_{\alpha} \cdot \mathbf{f}}}{1 - e^{-\beta N_{\alpha} \mathbf{a}_{\alpha} \cdot \mathbf{f}}} \right) e^{-\beta \mathbf{x}_n \cdot \mathbf{f}} \hat{\boldsymbol{\pi}}, \quad (6)$$

which reduces to (4) as  $|\mathbf{f}| \rightarrow 0$ . Under the widely used midpoint rule, the modified rate matrices are given by

$$\mathbf{Q}(\mathbf{d}, \mathbf{f}) \simeq \exp(-\beta \mathbf{d} \cdot \mathbf{f}/2) \mathbf{Q}(\mathbf{d}), \quad (7)$$

which clearly satisfies (5).

### A. Continuum Limit

The continuum limit of (1) is defined under the assumption that occupation probabilities vary slowly on the length scale of a single unit cell. In the next section, where we use Bloch's theorem to diagonalise (1), this is equivalent to only considering long-wavelength

modes. In this limit, we can equate the cell probability vector  $\mathbf{p}(\mathbf{x}_n, t)$  to a continuous (vector) probability density  $\boldsymbol{\rho}(\mathbf{x}, t)$ , which varies slowly over a unit cell of volume  $V = \mathbf{a}_0 \cdot (\mathbf{a}_1 \times \mathbf{a}_2)$ , giving

$$\mathbf{p}(\mathbf{x}_n, t) \rightarrow \boldsymbol{\rho}(\mathbf{x}, t) V d^3 \mathbf{x}. \quad (8)$$

Under the same assumption of slow variation, we make a Taylor expansion of  $\boldsymbol{\rho}(\mathbf{x}, t)$  to second order. The master equation (1) becomes the reaction-diffusion equation

$$\frac{d}{dt} \boldsymbol{\rho}(\mathbf{x}, t) = \mathbb{Q} \boldsymbol{\rho}(\mathbf{x}, t) + \mathbb{C} \boldsymbol{\rho}(\mathbf{x}, t) + \mathbb{D} \boldsymbol{\rho}(\mathbf{x}, t), \quad (9)$$

where, the reaction, drift and diffusion terms read

$$\mathbb{Q} = \mathbf{Q}(\mathbf{0}) + \sum_{\mathbf{d} \in \mathcal{T}} \mathbf{Q}(\mathbf{d}) - \mathbf{R}, \quad (10)$$

$$\mathbb{C} = \sum_{\mathbf{d} \in \mathcal{T}} \mathbf{Q}(\mathbf{d}) (\mathbf{d} \cdot \boldsymbol{\nabla}), \quad (11)$$

$$\mathbb{D} = \frac{1}{2} \sum_{\mathbf{d} \in \mathcal{T}} \mathbf{Q}(\mathbf{d}) (\mathbf{d} \cdot \boldsymbol{\nabla})^2. \quad (12)$$

The master equation (1) and its continuum limit (9) are the central equations of this paper.

We note that conventional reaction-diffusion equations assume the drift term  $\mathbb{C} \boldsymbol{\rho}$  to vanish; however, this is only true when a local cell-wise equilibrium approximation  $\boldsymbol{\rho}(\mathbf{x}, t) \simeq \hat{\boldsymbol{\pi}} \rho(\mathbf{x}, t)$  is valid and detailed balance holds, as we show below. In the general case,  $\mathbb{C} \boldsymbol{\rho}$  can play an important role in non-equilibrium mixing physics. In the examples below we demonstrate that these drift terms can be of greater magnitude than the pure reaction rates.

## III. SIMPLIFYING THE MASTER EQUATION

As discussed in the introduction, whilst the master equation (1) is exact under suitable limits, the number of states  $M$  can be very large, and the rate matrices can have widely varying rates, potentially introducing severe stability constraints on the integration timestep. This complexity will similarly affect the continuum limit (9).

In this section, we first use Bloch's theorem<sup>46</sup> to derive a closed form for the eigenmodes of the master equation (1), requiring only the diagonalization of small  $M \times M$  matrices, returning eigenvectors and eigenvalues which can naturally be indexed with respect to a reciprocal space vector  $\mathbf{k}$  in the first Brillouin zone and a 'band' index  $m \in [1, M]$ . Access to all the eigenvalues then allows us to look for gaps in the eigenvalue spectrum, with all above-gap modes considered 'fast' as they decay on a timescale where 'slow' modes are essentially constant. By removing the 'fast' modes we produce an effective master equation with a smaller number of states in each cell, equal to the number of retained bands, with a much narrower range of intrinsic timescales.

In cases where we find only one state per cell, this procedure results in a simple anisotropic diffusion equation.

In the general case, where a spectral gap may not be observed, we provide a solution for the continuum limit (9), which is equivalent to only considering the dynamics of long wavelength modes  $|\mathbf{k}| \rightarrow 0$ . We show that the long-wavelength spectrum often reveals effective spectral gaps at the cost of reduced spatial resolution, which we use to produce well-conditioned continuum equations.

### A. Eigenmodes of the master equation

As each cell probability vector  $\mathbf{p}(\mathbf{x}_n)$  is coupled to neighboring cells in the master equation (1), the effective transition rate matrix is of infinite dimension for an infinite system. However, due to the periodic translation symmetry, a solvable form of (1) can be obtained using Bloch's theorem<sup>46</sup>. We first define lattice translation operators

$$\hat{\mathbf{T}}(\mathbf{x}_m)\mathbf{p}(\mathbf{x}_n) \equiv \mathbf{p}(\mathbf{x}_n + \mathbf{x}_m), \quad (13)$$

to write the master equation (1) in the operator form

$$\frac{d}{dt}\mathbf{p}(\mathbf{x}_n) = \hat{\mathbf{Q}}\mathbf{p}(\mathbf{x}_n), \quad \hat{\mathbf{Q}} \equiv \mathbf{Q}(\mathbf{0}) - \mathbf{R} + \sum_{\mathbf{d} \in \mathcal{T}} \mathbf{Q}(\mathbf{d})\hat{\mathbf{T}}(\mathbf{d}).$$

Our goal is to find the (negated) eigenvalues and eigenfunctions

$$\hat{\mathbf{Q}}\mathbf{v}(\mathbf{x}_n) = -\lambda\mathbf{v}(\mathbf{x}_n), \quad \mathbf{v}(\mathbf{x}_n, t) = \exp(-\lambda t)\mathbf{v}(\mathbf{x}_n), \quad (14)$$

where definition of the sign of  $\lambda$  reflects the fact that  $\lambda \geq 0$  for physical Master equations.

As  $\hat{\mathbf{Q}}$  clearly commutes with any combination of  $\hat{\mathbf{T}}(\mathbf{d})$ , its vector-valued eigenfunctions satisfy a Bloch relation<sup>46</sup>

$$\mathbf{v}_{m\mathbf{k}}(\mathbf{x}_n) \equiv \exp(i\mathbf{x}_n \cdot \mathbf{k})\tilde{\mathbf{v}}_{m\mathbf{k}}, \quad (15)$$

where  $m \in [1, M]$ ,  $\mathbf{k}$  is a wavevector in the first Brillouin zone of the lattice defined by  $\mathcal{T}$ , and  $\tilde{\mathbf{v}}_{m\mathbf{k}} \in \mathbb{R}^M$  is constant across cells (but not within). The eigenvalue problem reduces to

$$\tilde{\mathbf{Q}}(\mathbf{k})\tilde{\mathbf{v}}_{m\mathbf{k}} = -\lambda_{m\mathbf{k}}\tilde{\mathbf{v}}_{m\mathbf{k}}, \quad (16)$$

where the  $M \times M$  'Bloch' transition matrix  $\tilde{\mathbf{Q}}(\mathbf{k})$  writes

$$\tilde{\mathbf{Q}}(\mathbf{k}) \equiv \mathbf{Q}(\mathbf{0}) - \mathbf{R} + \sum_{\mathbf{d} \in \mathcal{T}} \mathbf{Q}(\mathbf{d})\exp(i\mathbf{d} \cdot \mathbf{k}). \quad (17)$$

Computation of eigenvalues and eigenmodes therefore requires diagonalizing an  $M \times M$  matrix  $\tilde{\mathbf{Q}}(\mathbf{k})$  across some discrete grid of  $\mathbf{k}$ -points in the first Brillouin zone, in close analogy to Kohn-Sham density functional theory<sup>41</sup>.

This procedure will return right eigenvectors  $\tilde{\mathbf{v}}_{m\mathbf{k}}$  and eigenvalues  $\lambda_{m\mathbf{k}}$  as defined above, in addition to left eigenvectors  $\tilde{\mathbf{w}}_{m\mathbf{k}}$ , which satisfy the generalized orthogonality condition  $\tilde{\mathbf{w}}_{n\mathbf{k}} \cdot \tilde{\mathbf{v}}_{m\mathbf{k}} = \delta_{nm}$ . The master equation has left Bloch eigenvectors  $\mathbf{w}_{m\mathbf{k}}(\mathbf{x}_n) = \exp(-i\mathbf{x}_n \cdot \mathbf{k})\tilde{\mathbf{w}}_{m\mathbf{k}}$ ,

such that  $\sum_{\mathbf{x}_n} \mathbf{w}_{n\mathbf{k}'}(\mathbf{x}_n) \cdot \mathbf{v}_{m\mathbf{k}}(\mathbf{x}_n) = N_V \delta_{nm} \delta_{\mathbf{k}'\mathbf{k}}$ , where  $N_V$  is the total number of cells in the system.

The general time evolution of probability then reads

$$\mathbf{p}(\mathbf{x}_n, t) = \sum_{\mathbf{k}, m} a_{m\mathbf{k}} \mathbf{v}_{m\mathbf{k}}(\mathbf{x}_n, t), \quad (18)$$

where  $\mathbf{v}_{m\mathbf{k}}(\mathbf{x}_n, t) = \mathbf{v}_{m\mathbf{k}}(\mathbf{x}_n) \exp(-\lambda_{m\mathbf{k}} t)$  and  $a_{m\mathbf{k}} = \sum_{\mathbf{x}_n} \mathbf{w}_{m\mathbf{k}}(\mathbf{x}_n) \cdot \mathbf{p}(\mathbf{x}_n, 0)$ . As probability distributions are real, it is simple to show that  $a_{m, -\mathbf{k}}^\dagger = a_{m\mathbf{k}}$ . The steady state has eigenvalue  $\lambda_{00} = 0$ , with cell eigenvectors<sup>47</sup>

$$\tilde{\mathbf{w}}_{00} = \mathbf{1}, \quad \tilde{\mathbf{v}}_{00} = \hat{\boldsymbol{\pi}}, \quad a_{00} = \left( \prod_{\alpha} N_{\alpha} \right)^{-1}, \quad (19)$$

in agreement with (4).

#### 1. External driving force

The Bloch relation (15) derives from the general form of the eigenfunctions of the  $\hat{\mathbf{T}}(\mathbf{d})$ . As these periodic translation operators form a representation of the cyclic group<sup>48</sup>, it can be shown that the eigenvalues must be  $M$ -fold degenerate and be a scalar representation of the cyclic group, namely phase factors  $\exp(i\mathbf{d} \cdot \mathbf{k})$ .

In the presence of an external driving force  $\mathbf{f}$ , the modified detailed balance relations (5) imply that  $\hat{\mathbf{Q}}$  now commutes with  $\exp(-\beta\mathbf{d} \cdot \mathbf{f})\hat{\mathbf{T}}(\mathbf{d})$ . As the scalars  $\phi(\mathbf{d}) = \exp(-\beta\mathbf{d} \cdot \mathbf{f})$  have exactly the same commutation relations as the  $\hat{\mathbf{T}}(\mathbf{d})$ , the eigenfunctions of this modified operator are of exactly the same form, except that the phase factor also accounts for the energy difference due to  $\mathbf{f}$ , giving a generalized Bloch relation

$$\mathbf{v}_{m\mathbf{k}}(\mathbf{x}_n) \equiv \exp(\mathbf{x}_n \cdot [i\mathbf{k} - \beta\mathbf{f}])\tilde{\mathbf{v}}_{m\mathbf{k}}. \quad (20)$$

The full eigenspectrum can be found by solving the eigenvalue problem (16) as above, with suitably modified rate matrices satisfying (5).

### B. Spectral coarse-graining

The general principle behind spectral coarse-graining is to look for a spectral gap in the ordered list of (negated) eigenvalues  $\{\lambda_{m\mathbf{k}}\}$ . Aside from the steady state  $\lambda_{00} = 0$ , all modes are exponentially decaying with  $\lambda_{m\mathbf{k}} > 0$ . For any timescale  $\tau$ , we are free to define a (possibly vanishing) spectral gap  $\Delta_{\tau} > 0$  through

$$\Delta_{\tau} \equiv \left( \min_{\lambda_{m\mathbf{k}}\tau \geq 1} \lambda_{m\mathbf{k}} \right) - \left( \max_{\lambda_{m\mathbf{k}}\tau < 1} \lambda_{m\mathbf{k}} \right). \quad (21)$$

After a time  $t \sim \tau$  the general expansion (18) reads

$$\mathbf{p}(\mathbf{x}_n, t) \rightarrow \sum_{\lambda_{m\mathbf{k}}\tau < 1} a_{m\mathbf{k}} \mathbf{v}_{m\mathbf{k}}(\mathbf{x}_n, t) + \mathcal{O}(\exp(-\tau\Delta_{\tau})).$$

If  $\tau\Delta_\tau \gg 1$ , the reduced order model formed from below-gap modes will therefore have exponentially small error with respect to the true dynamics. If the number of below-gap modes is small, the reduced order model is typically much better suited for continuum implementation. Our objective is therefore to find conditions under which such a gap exists.

### C. Continuum limit in reciprocal space

The continuum limit (9) is defined to apply only to probability densities which are initialized to be slowly varying on the length-scale of a unit cell. From the Bloch relation (15), it is clear that this is equivalent to only considering contributions from eigenmodes of long spatial wavelength, where  $|\mathbf{k} \cdot \mathbf{d}| \ll 1$ . To produce a well-conditioned continuum equation, we thus do not need to have a spectral gap in the entire eigenmode distribution. We can instead focus on the  $M$  bands  $\lambda_{m\mathbf{k}}, m \in [1, M]$ , and look for the long wavelength spectral gap

$$\lambda_{(P+1)\mathbf{k}} \gg \lambda_{P\mathbf{k}}, \quad |\mathbf{k} \cdot \mathbf{d}| \ll 1. \quad (22)$$

To determine the spatial resolution more precisely, we can use first order perturbation theory to evaluate the long wavelength eigenvalue approximation

$$\lambda_{m\mathbf{k}} \simeq \lambda_{m\mathbf{k}}^0 = -\tilde{\mathbf{w}}_{m\mathbf{0}}^\top \tilde{\mathbf{Q}}(\mathbf{k}) \tilde{\mathbf{v}}_{m\mathbf{0}}, \quad |\mathbf{k} \cdot \mathbf{d}| \ll 1, \quad (23)$$

where  $\{\tilde{\mathbf{w}}_{m\mathbf{0}}, \tilde{\mathbf{v}}_{m\mathbf{0}}\}$  form the  $\mathbf{k} = \mathbf{0}$  basis. An appropriate grid size  $L$  can then be determined through the error measure

$$|\lambda_{m\mathbf{k}^L}^0 - \lambda_{m\mathbf{k}^L}| = \epsilon |\lambda_{m\mathbf{k}^L}|, \quad |\mathbf{k}^L \cdot \mathbf{1}|_\infty = \frac{\pi}{L}, \quad (24)$$

where  $|\mathbf{x}|_\infty \equiv \max(|x_0|, |x_1|, \dots)$ . If such a gap exists, we can produce an accurate reaction-diffusion equation from a reduced number states per cell, equal to the number of retained bands,  $P < M$ , with a corresponding compression in the range of inherent timescales, which makes time integration significantly more efficient.

### D. Building coarse-grained states with PCCA+

To determine the coarse grained states, we wish to partition the  $M$  states into  $P$  groups such that the intergroup transition rates are minimized, to ensure the timescale compression. This is a common objective in Markov model analysis; a popular approach, used here, is the Robust Perron Cluster Analysis (PCCA+) technique<sup>43</sup>, which is widely used in the biochemical community<sup>40</sup>. Whilst the original PCCA method<sup>42</sup> attempts to find a strict (non-overlapping) partitioning of the  $M$  states into  $P$  coarse-grained states, the PCCA+ technique instead forms ‘fuzzy’ clusters from linear combinations of the  $P$  slow eigenmodes. This is ideal for our usage, as we can then construct coarse-grained transition

state matrices for use in the continuum limit (9). We employ a python implementation of the PCCA+ algorithm from the `MSMTools` package<sup>49</sup>.

To define our coarse-grained states, we first form matrices of the slow eigenvectors

$$\begin{aligned} \mathbf{W}_P &\equiv [\tilde{\mathbf{w}}_{00}, \dots, \tilde{\mathbf{w}}_{P-1,0}] \in \mathbb{R}^{P \times M}, \\ \mathbf{V}_P &\equiv [\tilde{\mathbf{v}}_{00}, \dots, \tilde{\mathbf{v}}_{P-1,0}] \in \mathbb{R}^{P \times M}, \end{aligned} \quad (25)$$

The PCCA+ algorithm is then used to build the  $P \times P$  clustering matrix of linear coefficients

$$\mathbf{M}_P = \text{PCCA+}(\mathbf{Q}(\mathbf{0})) \in \mathbb{R}^{P \times P}, \quad (26)$$

which gives a coarse-grained probability vector

$$\boldsymbol{\rho}_P(\mathbf{x}, t) \equiv \mathbf{M}_P \mathbf{W}_P \boldsymbol{\rho} \in \mathbb{R}^P, \quad (27)$$

with coarse grained transition matrices

$$\mathbf{Q}_P(\mathbf{d}) \equiv \mathbf{M}_P \mathbf{W}_P \mathbf{Q}(\mathbf{d}) \mathbf{V}_P^\top \mathbf{M}_P^\top, \quad (28)$$

from which we can build a coarse grained reaction-diffusion equation operators  $\mathbb{Q}_P, \mathbb{C}_P, \mathbb{D}_P$ , in direct analogy with (9)

$$\frac{\partial}{\partial t} \boldsymbol{\rho}_P(\mathbf{x}, t) = \mathbb{Q}_P \boldsymbol{\rho}_P + \mathbb{C}_P \boldsymbol{\rho}_P + \mathbb{D}_P \boldsymbol{\rho}_P. \quad (29)$$

In the next section, we apply this methodology to illustrative examples.

## IV. EXAMPLE APPLICATIONS

### A. Simplest case: local equilibrium, $P=1$

We first treat the simplest case, where the lowest eigenvalue band is well separated from all the others, corresponding to the case where intracell transitions are much faster than intercell transitions. The left and right eigenvectors  $\tilde{\mathbf{w}}_{0\mathbf{k}}, \tilde{\mathbf{v}}_{0\mathbf{k}}$  will be to a high degree of approximation the steady state vectors  $\mathbf{1}, \hat{\boldsymbol{\pi}}$  for all values of  $\mathbf{k}$ , meaning the slow eigenmodes can be written

$$\tilde{\mathbf{w}}_{0\mathbf{k}} \simeq \mathbf{1}, \quad \tilde{\mathbf{v}}_{0\mathbf{k}} \simeq \hat{\boldsymbol{\pi}},$$

where these relations become exact in the limit of vanishing intercell transitions rates. As we have only one cluster, our reduced probability density is the scalar

$$\rho_P(\mathbf{x}, t) = \mathbf{1} \cdot \boldsymbol{\rho}(\mathbf{x}, t), \quad (30)$$

which is clearly a local equilibrium approximation. This immediately implies that the reaction term vanishes-

$$\mathbb{Q}_P \rho_P(\mathbf{x}, t) = \mathbf{1}^\top \left[ \sum_{\mathbf{d} \in \mathcal{T}} \mathbf{Q}(\mathbf{d}) - \mathbf{R} \right] \hat{\boldsymbol{\pi}} \rho(\mathbf{x}, t) = 0. \quad (31)$$

The long wavelength approximation (23) is then highly accurate, with eigenvalues of the form

$$\lambda_{0\mathbf{k}} \simeq \lambda_{0\mathbf{k}}^0 = \sum_{\mathbf{d} \in \mathcal{T}} 2 \sin^2(\mathbf{d} \cdot \mathbf{k}) (\mathbf{1}^\top \mathbf{Q}(\mathbf{d}) \hat{\boldsymbol{\pi}}). \quad (32)$$

As mentioned above, the drift term vanishes due to the detailed balance symmetry (3)

$$\mathbb{C}_{P\rho P}(\mathbf{x}, t) = \frac{1}{2} \sum_{\mathbf{d} \in \mathcal{T}} \mathbf{1}^\top (\mathbf{Q}(\mathbf{d}) - \mathbf{Q}(-\mathbf{d})) \hat{\boldsymbol{\pi}} \mathbf{d} \cdot \nabla \rho_P = 0,$$

whilst the diffusion operator acts only on the scalar probability density  $\rho(\mathbf{x}, t)$

$$\mathbb{D}_{P\rho P}(\mathbf{x}, t) = \nabla \cdot \mathbf{D} \cdot \nabla \rho_P(\mathbf{x}, t). \quad (33)$$

We can therefore take the continuum limit (9) for  $\rho$ , which has the pure diffusion form

$$\frac{d}{dt} \rho(\mathbf{x}, t) = \nabla \cdot \mathbf{D} \cdot \nabla \rho(\mathbf{x}, t) \quad (34)$$

where the  $3 \times 3$  diffusion matrix reads, from (9),

$$\mathbf{D} = \frac{1}{2} \sum_{\mathbf{d} \in \mathcal{T}} (\mathbf{1}^\top \mathbf{Q}(\mathbf{d}) \hat{\boldsymbol{\pi}}) \mathbf{d} \mathbf{d}^\top. \quad (35)$$

For sufficiently symmetric defects the diffusion matrix can reduce to  $\mathbf{D} = D\mathbb{I}$ , giving the familiar isotropic diffusion equation  $(d/dt)\rho = D\nabla^2\rho$ . An example of such a system is shown in figure 1a, where we have labeled the transition matrices  $\mathbf{Q}(\mathbf{d})$ .

### B. Long wavelength spectral gap: $P=1$

As a slightly more complex case, consider the system in figure 1b, which has a clear separation of timescales for migration in one direction but competing timescales for mixing and migration in the other. However, for the continuum equation, we can ‘create’ a spectral gap by setting the spatial resolution through an upper bound on  $\mathbf{k}$ , such that the largest permitted mode of the highest retained band still has a well defined gap to the lowest mode of the next band. A larger gap, and thus a lower error in the propagated density, can be found by sacrificing spatial resolution, offering a simple trade-off depending on the desired application. In the case presented in figure 1b we recover the same simple diffusion form as presented in (35), but with a highly anisotropic diffusivity.

### C. Multistate reaction-diffusion : $P=2$

We now consider additional structure in the model, designed to return a two-state reaction-diffusion equation. The inter-cell transitions split into two super-basins, with one super-basin having fast migration along  $\hat{\mathbf{x}}$ , and the

other having fast migration along  $\hat{\mathbf{y}}$ . The long-time behaviour is thus isotropic, but the short-time behaviour is anisotropic. A physical example of such a system is the crowdion self-interstitial defect found in some body centered cubic metals<sup>50,51</sup>, which executes long periods of fast one dimensional migration along a given  $\langle 111 \rangle$  direction, punctuated by rare rotations between different symmetry-equivalent directions.

With  $P$  (in this example  $P = 2$ ) retained bands, we construct an effective coarse-grained system of  $P$  effective states using the PCCA+ technique described above. However, in the present simplified example the PCCA+ clustering can be performed analytically in the limit of strongly metastable superbins, where the second-lowest left eigenvector  $\tilde{\mathbf{w}}_{10}$  will be approximately  $-1$  in one basin and  $1$  in the other. As  $\tilde{\mathbf{w}}_{00} = \mathbf{1}$  is constant, we can then select one basin with  $(\tilde{\mathbf{w}}_{00} + \tilde{\mathbf{w}}_{10})/2$  and the other with  $(\tilde{\mathbf{w}}_{00} - \tilde{\mathbf{w}}_{10})/2$ , giving an approximate clustering matrix

$$\mathbf{M}_P \simeq \frac{1}{2} \begin{bmatrix} 1 & 1 \\ -1 & 1 \end{bmatrix}. \quad (36)$$

This form is can be expected for strongly metastable dynamics when  $P = 2$ .

To investigate the form of the resultant continuum equation, we expand the reduced reaction, drift and diffusion operators into  $2 \times 2$  matrix-valued coefficients

$$\mathbb{Q}_{P\rho P} = \mathbf{Q}_P \rho_P, \quad \mathbb{C}_{P\rho P} = \sum_{\alpha} \mathbf{C}_{\alpha} \frac{\partial}{\partial x_{\alpha}} \rho_P \quad (37)$$

$$\mathbb{D}_{P\rho P} = \sum_{\alpha, \alpha'} \mathbf{D}_{\alpha\alpha'} \frac{\partial^2}{\partial x_{\alpha} \partial x_{\alpha'}} \rho_P. \quad (38)$$

by carrying out the sums over the primitive set of translations  $\mathcal{T}$  in the coarse-grained versions of Eq. 12 and gathering the terms corresponding to the same derivatives. From the form of the model presented in figure (1), one can expect that the diffusion coefficients  $\mathbf{D}_{\alpha\alpha'}$  will have the largest components, due to the fast migration directions along either  $\mathbf{x}$  or  $\mathbf{y}$ .

However, to change migration direction, the system must execute a inter-basin transition (i.e. between coarse grained states), either in the same cell, as governed by the off-diagonal components of  $\mathbf{Q}_P$ ,  $\mathbf{C}_{\alpha}$  and  $\mathbf{D}_{\alpha\alpha'}$ . In figure 2 we plot these coefficient matrices for the reaction operator and drift or diffusion along  $\mathbf{x}$ . As can be seen, the diffusion matrix has essentially one non-zero component, on the diagonal, corresponding to transitions between periodically equivalent coarse-grained states. Notably, the drift operator, missing in standard derivations of reaction-diffusion equations, is of greater magnitude than the coefficients in the reaction matrix, showing that these terms must not be neglected in general when building multi-state reaction-diffusion equations.

## V. CONCLUSIONS

In this paper, we have developed a comprehensive and efficient approach to coarse-grain complex periodic continuum Markov chains into compact, accurate, and numerically efficient continuum reaction-drift-diffusion equations. To do so, we calculate the eigenmodes of general master equations for materials defects employing a generalized Bloch theorem. Access to this spectrum is then used with an established kinetic clustering routine, the PCCA+ method<sup>43</sup>, to build well-conditioned continuum reaction-drift-diffusion equations. In future work this methodology will be applied to data from atomic sampling and implemented in mesoscale modeling schemes.

## VI. CODE AVAILABILITY

Code to generate the figures can be found at [github.com/tomswinburne/ReactionDiffusion](https://github.com/tomswinburne/ReactionDiffusion).

## VII. ACKNOWLEDGEMENTS

TDS gratefully recognizes support from the Agence Nationale de Recherche, via the MEMOPAS project ANR-19-CE46-0006-1. This work was granted access to the HPC resources of IDRIS under the allocation A0090910965 attributed by GENCI, and has been carried out within the framework of the EUROfusion consortium and has received funding from the Euratom research and training programme 2019-2020 under grant agreement No 633053. The views and opinions expressed herein do not necessarily reflect those of the European Commission. DP was supported by the Laboratory Directed Research and Development program of Los Alamos National Laboratory under project number 20220063DR. Los Alamos National Laboratory is operated by Triad National Security LLC, for the National Nuclear Security administration of the U.S. DOE under Contract No. 89233218CNA0000001.

- 
- \* [swinburne@cinam.univ-mrs.fr](mailto:swinburne@cinam.univ-mrs.fr)
- <sup>1</sup> L. Kubin, *Dislocations, Mesoscale Simulations and Plastic Flow*, Oxford Series on Materials Modelling (OUP Oxford, 2013).
  - <sup>2</sup> L. Dezerald, L. Proville, L. Ventelon, F. Willaime, and D. Rodney, *Physical Review B* **91**, 094105 (2015).
  - <sup>3</sup> T. D. Swinburne, K. Arakawa, H. Mori, H. Yasuda, M. Ishiki, K. Mimura, M. Uchikoshi, and S. L. Dudarev, *Scientific Reports* **6** (2016).
  - <sup>4</sup> R. Alexander, M.-C. Marinica, L. Proville, F. Willaime, K. Arakawa, M. Gilbert, and S. Dudarev, *Physical Review B* **94**, 024103 (2016).
  - <sup>5</sup> M. R. Sorensen, Y. Mishin, and A. F. Voter, *Phys. Rev. B* **62**, 3658 (2000).
  - <sup>6</sup> B. Uberuaga, R. Smith, A. Cleave, G. Henkelman, R. Grimes, A. Voter, and K. Sickafus, *Nuclear Instruments and Methods in Physics Research Section B: Beam Interactions with Materials and Atoms* **228**, 260 (2005).
  - <sup>7</sup> B. Uberuaga, R. Hoagland, A. Voter, and S. Valone, *Physical review letters* **99**, 135501 (2007).
  - <sup>8</sup> D. Perez, B. P. Uberuaga, Y. Shim, J. G. Amar, and A. F. Voter, *Annual Reports in computational chemistry* **5**, 79 (2009).
  - <sup>9</sup> L. K. Béland, P. Brommer, F. El-Mellouhi, J.-F. Joly, and N. Mousseau, *Physical Review E* **84**, 046704 (2011).
  - <sup>10</sup> A. F. Voter, *Physical Review Letters* **78**, 3908 (1997).
  - <sup>11</sup> A. F. Voter, *Physical Review B* **57**, R13985 (1998).
  - <sup>12</sup> M. So and A. Voter, *The Journal of Chemical Physics* **112**, 9599 (2000).
  - <sup>13</sup> A. Chatterjee and S. Bhattacharya, *The Journal of Chemical Physics* **143**, 114109 (2015).
  - <sup>14</sup> S. T. Chill and G. Henkelman, *The Journal of chemical physics* **140**, 214110 (2014).
  - <sup>15</sup> T. D. Swinburne and D. Perez, *Phys. Rev. Materials* **2**, 053802 (2018).
  - <sup>16</sup> T. D. Swinburne and D. Perez, *NPJ Computational Materials* **6**, 190 (2020).
  - <sup>17</sup> G. Henkelman and H. Jónsson, *The Journal of chemical physics* **111**, 7010 (1999).
  - <sup>18</sup> D. J. Wales, *Molecular physics* **100**, 3285 (2002).
  - <sup>19</sup> T. Lelièvre, “Mathematical foundations of accelerated molecular dynamics methods,” in *Handbook of Materials Modeling : Methods: Theory and Modeling*, edited by W. Andreoni and S. Yip (Springer International Publishing, Cham, 2018) pp. 1–32.
  - <sup>20</sup> G. Henkelman, *Annual Review of Materials Research* (2017).
  - <sup>21</sup> C. Le Bris, T. Lelièvre, M. Luskin, and D. Perez, *Monte Carlo Methods and Applications* **18**, 119 (2012).
  - <sup>22</sup> T. Swinburne and D. Perez, “**TAMBER** branch of **ParSplice** code,” (2018).
  - <sup>23</sup> T. D. Swinburne, *Computational Materials Science* **193**, 110256 (2021).
  - <sup>24</sup> T. Opplestrup, V. V. Bulatov, G. H. Gilmer, M. H. Kalos, and B. Sadigh, *Physical review letters* **97**, 230602 (2006).
  - <sup>25</sup> M. Athenes, S. Kaur, G. Adjanor, T. Vanacker, and T. Jourdan, *Physical Review Materials* **3**, 103802 (2019).
  - <sup>26</sup> T. Jourdan, G. Bencteux, and G. Adjanor, *Journal of Nuclear Materials* **444**, 298 (2014).
  - <sup>27</sup> T. Jourdan, *Journal of Nuclear Materials* **467**, 286 (2015).
  - <sup>28</sup> S. Blondel, D. E. Bernholdt, K. D. Hammond, L. Hu, D. Maroudas, and B. D. Wirth, *Fusion Science and Technology* **71**, 84 (2017).

- <sup>29</sup> A. Donev, V. V. Bulatov, T. Opperstrup, G. H. Gilmer, B. Sadigh, and M. H. Kalos, *Journal of Computational Physics* **229**, 3214 (2010).
- <sup>30</sup> D. R. Mason, X. Yi, M. A. Kirk, and S. L. Dudarev, *Journal of Physics: Condensed Matter* **26**, 375701 (2014).
- <sup>31</sup> T. Jourdan, *Modelling and Simulation in Materials Science and Engineering* **29**, 035007 (2021).
- <sup>32</sup> G. Demange, L. Lunéville, V. Pontikis, and D. Simeone, *Journal of Applied Physics* **121**, 125108 (2017).
- <sup>33</sup> M. Noble, M. Tonks, and S. Fitzgerald, *Physical review letters* **124**, 167401 (2020).
- <sup>34</sup> Y. Li, M. Boleininger, C. Robertson, L. Dupuy, and S. L. Dudarev, *Physical Review Materials* **3**, 073805 (2019).
- <sup>35</sup> Y. Li, G. Po, and N. Ghoniem, *Materialia* **14**, 100891 (2020).
- <sup>36</sup> Q. Yu, S. Chatterjee, K. J. Roche, G. Po, and J. Marian, *Modelling and Simulation in Materials Science and Engineering* **29**, 055021 (2021).
- <sup>37</sup> C. McElfresh, Y. Cui, S. L. Dudarev, G. Po, and J. Marian, *International Journal of Plasticity* **136**, 102848 (2021).
- <sup>38</sup> T. Swinburne and S. Dudarev, *Phys. Rev. Materials* **2**, 073608 (2018).
- <sup>39</sup> A. A. Kohnert, B. D. Wirth, and L. Capolungo, *Computational Materials Science* **149**, 442 (2018).
- <sup>40</sup> V. S. Pande, K. Beauchamp, and G. R. Bowman, *Methods* **52**, 99 (2010).
- <sup>41</sup> R. M. Martin, *Electronic Structure: Basic Theory and Practical Methods* (Cambridge University Press, 2004).
- <sup>42</sup> P. Deuffhard and M. Weber, *Linear algebra and its applications* **398**, 161 (2005).
- <sup>43</sup> S. Röblitz and M. Weber, *Advances in Data Analysis and Classification* **7**, 147 (2013).
- <sup>44</sup> T. S. Hudson, S. L. Dudarev, M. J. Catura, and A. P. Sutton, *Philosophical Magazine* **85**, 661 (2005).
- <sup>45</sup> L. E. Reichl, *A Modern Course in Statistical Physics*, *Physics Textbook* (Wiley-VCH, 2009).
- <sup>46</sup> N. W. Ashcroft and N. D. Mermin, *Solid state physics*, *Holt-Saunders International Editions: Science : Physics* (Holt, Rinehart and Winston, 1976).
- <sup>47</sup> T. D. Swinburne, D. Kannan, D. J. Sharpe, and D. J. Wales, *The Journal of Chemical Physics* **153**, 134115 (2020).
- <sup>48</sup> W. R. Scott, *Group theory* (Courier Corporation, 2012).
- <sup>49</sup> P. team, “**MSMTools package**,” (2020).
- <sup>50</sup> T. D. Swinburne, S. L. Dudarev, and A. P. Sutton, *Physical Review Letters* **113**, 215501 (2014).
- <sup>51</sup> T. D. Swinburne, P.-W. Ma, and S. L. Dudarev, *New Journal of Physics* **19**, 073024 (2017).

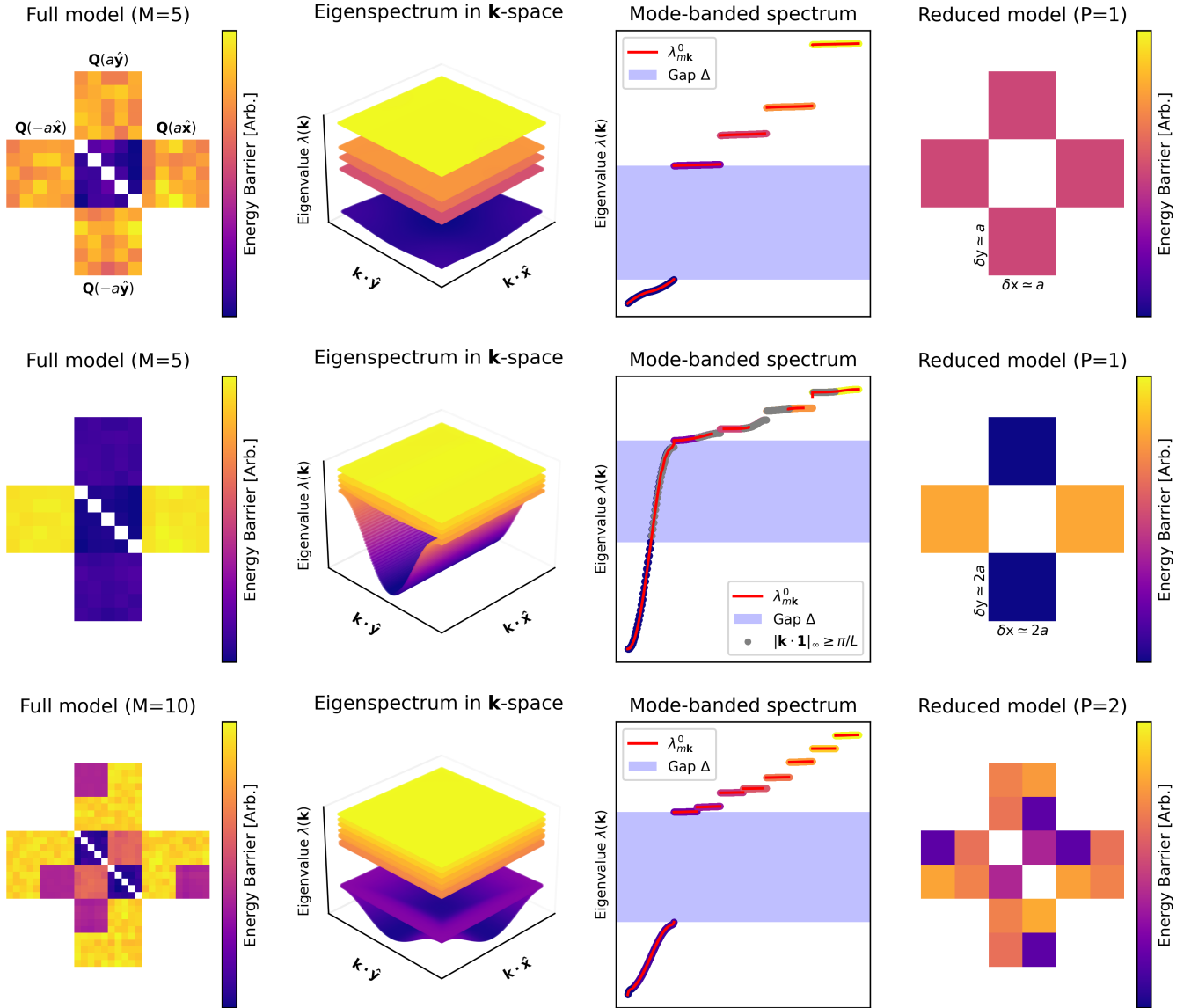


FIG. 1. Coarse graining of a model systems which diffuse in two dimensions. For simplicity we only consider nearest neighbor transitions. Top: A simple ‘mixing’ case, where local equilibrium is reached in the cell before any transitions. The full eigenspectrum has a clear gap; retaining only the slow modes returns a simple single state diffusion model. Middle: A more complex case, where the timescale for diffusion along  $\mathbf{y}$  is comparable to that of intercell mixing. Whilst the full spectrum is dense, we can find a gap in a restricted region of  $\mathbf{k}$ -space, corresponding to a coarser spatial resolution in the fast diffusion direction, returning a reduced order model. Bottom: A multi-state case, where the cell divides into two superbasins, each having fast migration kinetics along different directions. A spectral gap exists above the second band, returning a two state model with the PCCA+ procedure.

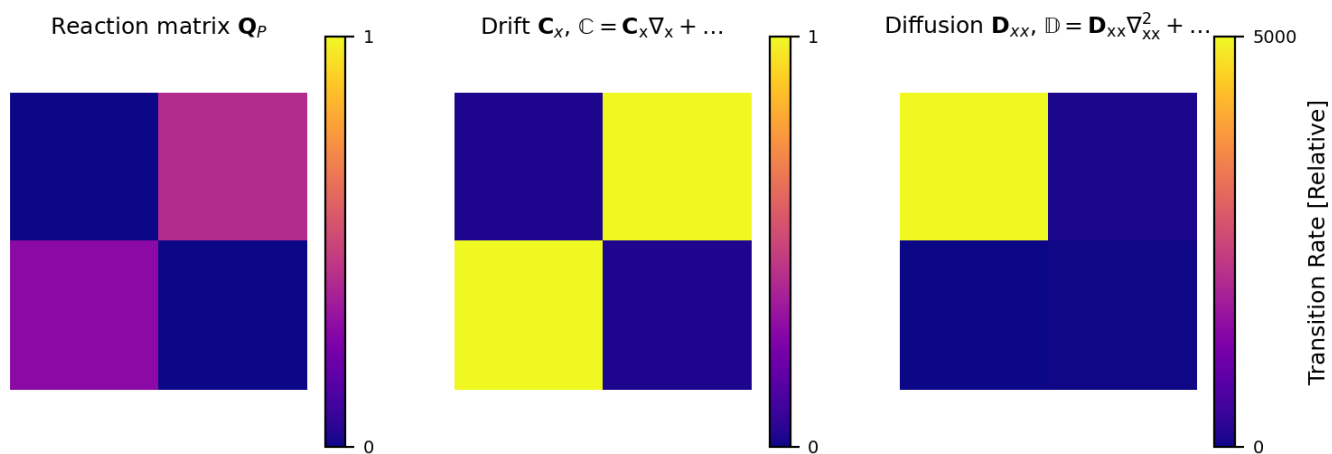


FIG. 2. Some matrix coefficients forming operators in the reaction-diffusion equation for the last example shown in figure 1. Matrix elements are colored on a relative scale to aid comparison. The drift coefficients are comparable in magnitude to the reaction terms, showing that the typically neglected drift operator  $\mathbb{C}$  is essential to capture the correct kinetics.